Quantum instanton evaluations of surface diffusion, interior migration, and surface-subsurface transport for H/Ni

Wenji Wang and Yi Zhao[a)]
Department of Chemistry, State Key Laboratory for Physical Chemistry of Solid Surfaces, College of Chemistry and Chemical Engineering, Xiamen University, Xiamen 361005, People's Republic of China and Department of Chemical Physics, University of Science and Technology of China, Hefei 230026, People's Republic of China

(Received 29 October 2009; accepted 23 January 2010; published online 11 February 2010)

The quantum instanton approximation is extended to investigate dynamical processes of hydrogen on surface, from surface to subsurface, and between interior sites in nickel lattice. The path integral Monte Carlo and adaptive umbrella sampling techniques are employed to manipulate the quantum instanton formula. The free energy profiles along reaction paths, temperature dependence of free energies, and rates as well as diffusion coefficients are calculated for each process. The results manifest that the motions of nickel atoms beneath the surface have little effect on the hydrogen diffusion on Ni(111), and the hydrogen at the fcc binding site is much easier to get into bulk nickel than the one at the hcp site. The temperature dependence of free energy profiles also reveals that the hydrogen in the subsurface octahedral vacancy and interior tetrahedral vacancy becomes unstable at low temperatures, which proposes a temperature dependence of reaction mechanism. In addition, the relaxations of the lattices dramatically lower the free energy barriers except for the process of the hydrogen diffusion on Ni(111). The quantum motions of the lattice atoms affect the free energies little at 300 K, but they hinder the rates by 20%–40% compared with the classical motions of lattice atoms. © *2010 American Institute of Physics*. [doi:10.1063/1.3317475]

I. INTRODUCTION

Hydrogen adsorption and diffusion on metal surface are of interest from scientific perspective of understanding the gas-surface interactions to the vast field heterogeneous catalysis, surface electronics, and energy storage. In addition, they provide the simplest model system for validating theoretical and experimental methodologies. In our previous paper,[1] the diffusion of hydrogen on Ni(100) surface is evaluated by using the quantum instanton (QI) approximation.[2] The QI has successfully revealed the tunneling effect, predicted the transition temperature, and explained the dissipation phenomenon caused by interaction between hydrogen and metallic atoms.

The QI is proposed recently by Miller *et al.*[2] for the calculations of reaction rates. Its approximation is similar to an earlier semiclassical transition state theory[3] that became known as the instanton.[4] However, it has the advantage that the Boltzmann operator is treated fully quantum mechanically rather than within the semiclassical approximation. Furthermore, the QI approximation only incorporates the calculations of the Boltzmann operator and its relevant quantities. It therefore allows one to calculate large systems quantum dynamically, together with path integral Monte Carlo (MC) and adaptive umbrella sampling techniques. For instance, 25 Ni atoms and the hydrogen have been dealt with full quantum mechanics for hydrogen diffusion on Ni(100).[1] Meanwhile, the QI considers all tunneling paths and automatically gives each path its natural weight by the quantum Boltzmann factor and incorporates quantum-fluctuation effect correctly. It can be manipulated in Cartesian space on a full potential energy surface, thus takes into account the effects of the vibration-rotation coupling and anharmonicity of the reaction system naturally. The previous applications from gas phase reactions[5–7] to proton transfer in a polar solvent[8] have also demonstrated its merits.

The present paper, which is an extension of our previous work,[1] continuously applies the QI approximation to investigate the hydrogen diffusion on Ni(111), as well as surface-subsurface processes and the migration between the interior sites. Concretely speaking, we calculate the rates for the cyclic reaction processes that H atom hops along the reversible path $A_{\mathrm{hcp}} \rightleftharpoons A_{\mathrm{fcc}} \rightleftharpoons Oc_{\mathrm{sub}} \rightleftharpoons Te_{\mathrm{sub}} \rightleftharpoons A_{\mathrm{hcp}}$ (see in Fig. 1), and H atom diffuses from one interior octahedral site to another via a tetrahedral site (see in Fig. 2).

The behaviors of hydrogen on metal surfaces considered in this paper have been investigated both experimentally and theoretically, as reviewed in several places.[9–17] Theoretically, most work is based on the adiabatic potential or the minimum energy path to calculate the rates with use of transition state theories because a rigorous multidimensional quantum dynamical calculation is still prohibitive at the moment. However, dynamics of the lattice may significantly contribute to the rates, as shown in the QI calculations of H diffusion on Ni(100) (Ref. 1) with use of a full-dimensional potential energy surface. The QI results show that the quantum lattice motion can hinder the hydrogen tunneling comparing with the classical ones. This result is in conflict with one from the variational transition state theory,[18] but consistent

[a)]Author to whom correspondence should be addressed. Electronic mail: yizhao@xmu.edu.cn.

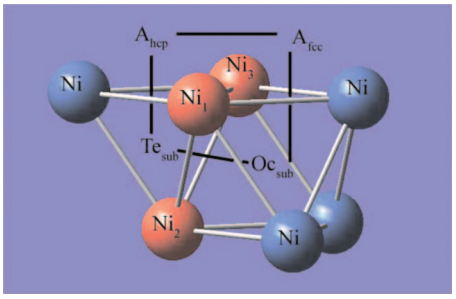

FIG. 1. A lattice model with a few Ni atoms for the circle reaction processes of hydrogen. A_{hcp}, A_{fcc}, Oc_{sub}, and Te_{sub} are the abbreviations for a hcp hollow site, a fcc hollow site, a subsurface octahedral vacancy, and a subsurface tetrahedral vacancy, respectively. The black lines stand for the directions of the reaction paths. The atoms of Ni_1, Ni_2, and Ni_3 colored in orange are specially used to determine the reaction coordinate of the process $Oc_{sub} \rightarrow Te_{sub}$.

with that from the surrogate Hamiltonian method.[19] The possible mechanism has been explained from both the free energy profile and the dissipative effect.[1]

For the processes of H diffusion on the Ni(111) crystal surface, H hopping between surface and subsurface sites, and H migrating in the interior, several theoretical investigations have also been made. For instance, Wonchoba and Truhlar[20] investigate the surface, subsurface, and interior processes using canonical variational transition state theory with a small curvature tunneling approximation based on quantized reactant states (CVT/SCTQ), or by treating the energy levels of the reaction coordinate as a classical continuum (CVT/SCT) on a full dimensional potential energy function, and they predicted that the quantum motion of lattice does not affect rates too much comparing with classical one. However, Baer *et al.*[21] use the surrogate Hamiltonian method to represent the nickel host effect on the hydrogen resurface dynamics and show that the environment suppresses the tunneling compared to a frozen lattice approximation, using their own potential energy function. This makes us expect that the quantum lattice may be also important for understanding the dynamics at subsurface and interior sites. Therefore, besides the study of circle kinetic steps, the present paper also focuses on this problem. In the calculations, the version 6 of

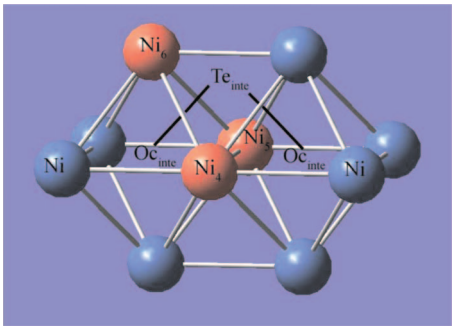

FIG. 2. A lattice model with a few Ni atoms for the process of H diffusion in interior of bulk Ni. Oc_{inte} and Te_{inte} are the abbreviations for an interior octahedral vacancy and an interior tetrahedral vacancy, respectively. The black lines stand for the general directions of the reaction paths. The atoms of Ni_4, Ni_5, and Ni_6 colored in orange are specially used to determine the reaction coordinate of the process $Oc_{inte} \rightarrow Te_{inte}$.

the embedded diatomics-in-molecules (EAM6) potential energy function[20] is used for the purpose of comparison with the CVT/SCTQ and CVT/SCT.

Another goal of the present paper is to reveal temperature dependence of quantum free energies, which may become important to determine the kinetic steps for the reactions in that a shallow potential well exists along reaction paths. An example is that H diffusion from one interior octahedral site to another via a tetrahedral site. Wonchoba and Truhlar[20] consider that the local minimum at tetrahedral site is not very deep, and treat the process as a single kinetic step with a double maximum barrier, while Wimmer *et al.*[22] assume that the diffusing H atom temporarily equilibrates in the tetrahedral site before jumping forward or backward to a neighboring octahedral site, and treat this process as two individual kinetic steps. The assumption is based on the potential energy curve where a well indeed exists at the tetrahedral site. In fact, the rates are determined by the free energy. The validity of the above assumption may be examined more reasonably by the free energy profile along the reaction path. Our calculation will show that the kinetic reaction steps may depend on temperature.

The paper begins in Sec. II with the summarization of the working expression of the QI theory and the description of the path integral framework for the evaluation of the QI rates. Section III shows the model for the potential energy function and the numerical techniques. Section IV gives out numerical results. Section V is the concluding remarks.

II. THEORY

A. QI approximation

In this section, we summarize the working expressions of the QI approximation. The detailed derivation can be found in Refs. 2, 5, and 6. The QI model proposes a thermal rate expression as follows:

$$kQ_r \approx \frac{\sqrt{\pi}\hbar}{2} \frac{C_{ff}(0)}{\Delta H(\beta)}. \tag{1}$$

Here, Q_r is the reactant partition function per unit volume. $C_{ff}(0)$ is the zero time value of the flux-flux correlation function

$$C_{ff}(t) = \mathrm{tr}[e^{-\beta\hat{H}/2}\hat{F}_a e^{-\beta\hat{H}/2} e^{i\hat{H}t/\hbar}\hat{F}_b e^{-i\hat{H}t/\hbar}], \tag{2}$$

where β is the inverse temperature $1/k_B T$, $\hat{H}$ is the Hamiltonian operator of the system

$$\hat{H} = \frac{\hat{p}^2}{2m} + \sum \frac{\hat{p}^2}{2M} + V(\hat{r},\hat{R}) \tag{3}$$

the coordinates, masses, and momenta corresponding to the H atom and Ni atoms are denoted with $\hat{r}$, m, $\hat{p}$, and $\hat{R}$, M, $\hat{P}$, respectively, and the flux operators, $\hat{F}_\alpha(\alpha=a,b)$, are given by

$$\hat{F}_\alpha = \frac{1}{2m}[\hat{p}_s \delta(\hat{s}-s_\alpha) + \delta(\hat{s}-s_\alpha)\hat{p}_s]. \tag{4}$$

Here, the coordinate operator $\hat{s}$ is defined as the reaction coordinate. $\hat{p}_s$ is the conjugate momentum operator of $\hat{s}$. The

dividing surfaces are defined as $s=s_\alpha(\alpha=a,b)$.

ΔH in Eq. (1) is a specific type of energy variance, given by

$$\Delta H = \hbar \sqrt{\frac{-\ddot{C}_{dd}(0)}{2C_{dd}(0)}}, \tag{5}$$

where $C_{dd}(0)$ and $\ddot{C}_{dd}(0)$ are the zero time value and its second time derivative, respectively, of the "delta-delta" correlation function

$$C_{dd}(t) = \mathrm{tr}[e^{-\beta\hat{H}/2}\delta(\hat{s}-s_a)e^{-\beta\hat{H}/2}e^{i\hat{H}t/\hbar}\delta(\hat{s}-s_b)e^{-i\hat{H}t/\hbar}]. \tag{6}$$

In practice, in order to correct the free particle (or high-temperature) limit, that has very little effect in the low temperature regime, one may modify ΔH as

$$\Delta H_{\mathrm{mod}} = \Delta H + \frac{\sqrt{\pi}-\sqrt{2}}{\beta}. \tag{7}$$

The location of the dividing surfaces, namely, the values of the parameter s_α, are determined by the following stationary condition

$$\frac{\partial}{\partial s_\alpha} C_{dd}(0) = 0. \tag{8}$$

This condition originates from the semiclassical instanton model, and the resulting dividing surfaces correspond qualitatively to the turning points of the periodic orbit that runs on the upside down potential energy surface in imaginary time.

B. Path integral evaluation of QI rates

The QI rates in Eq. (1) is expressed solely in terms of the Boltzmann operator, they can be readily evaluated using imaginary-time path integral MC (PIMC) (Refs. 23–25) techniques. The PIMC calculations for the relevant quantities, i.e., $C_{ff}(0)$, $C_{dd}(0)$, and ΔH have been discussed extensively in the previous work.[5,1] In the following, we will give a brief review.

Equation (1) can be written as the product of several ratios

$$k = \frac{\sqrt{\pi}\hbar}{2}\frac{C_{dd}(0)}{Q_r}\frac{C_{ff}(0)}{C_{dd}(0)}\frac{1}{\Delta H(\beta)} \tag{9}$$

for the purpose of MC calculations. Here, $C_{ff}(0)/C_{dd}(0)$ and $\Delta H(\beta)$ are straightforwardly evaluated by the PIMC technique, while the evaluation of $C_{dd}(0)/Q_r$ is dealt with the adaptive umbrella sampling technique.[26–28]

We now explicitly present these ratios of the QI rate for H/Ni systems in the path integral representation. All the path integral expressions are presented fully quantized for both H atom and Ni atoms that neighbor reaction path. The light hydrogen atom is treated with P time slices, while the heavy Ni atoms are treated with fewer P_{bath} time slices.

Following the procedure described in Refs. 8 and 1, we transform $C_{dd}(0)$ and $C_{ff}(0)$ into discretized path integral forms, then obtain

$$\frac{C_{ff}(0)}{C_{dd}(0)} = \left\langle \frac{-P^2}{4\hbar^2\beta^2}(s_1-s_{P-1})(s_{P/2+1}-s_{P/2-1})\right\rangle_{\ddagger}, \tag{10}$$

where $\langle\cdots\rangle_{\ddagger}$ represents the constrained path average

$$\langle\cdots\rangle_{\ddagger} = \frac{\int dr_1\cdots\int dr_P\int dR_1\cdots\int dR_{P_{\mathrm{bath}}}\exp\{-\beta\Phi\}\delta(s_0-s_a)\delta(s_{P/2}-s_b)(\cdots)}{\int dr_1\cdots\int dr_P\int dR_1\cdots\int dR_{P_{\mathrm{bath}}}\exp\{-\beta\Phi\}\delta(s_0-s_a)\delta(s_{P/2}-s_b)}, \tag{11}$$

with

$$\Phi = \frac{MP_{\mathrm{bath}}}{2\hbar^2\beta^2}\sum_{\sigma=1}^{P_{\mathrm{bath}}}(R_\sigma-R_{\sigma-1})^2 + \frac{mP}{2\hbar^2\beta^2}\sum_{k=1}^{P}(r_k-r_{k-1})^2 + \frac{1}{P}\sum_{k=1}^{P}V(r_k,R_{\sigma[k]}). \tag{12}$$

ΔH is obtained via Eq. (5) by first getting the terms $\ddot{C}_{dd}(0)/C_{dd}(0)$

$$\frac{\ddot{C}_{dd}(0)}{C_{dd}(0)} = -\frac{1}{\hbar^2}\langle F^2+G\rangle_{\ddagger}, \tag{13}$$

where

$$F = \sum_{k=1}^{P}\left\{\frac{m}{2\hbar^2\Delta\beta^2}(r_k-r_{k-1})^2 - \frac{1}{2}[V(r_k,R_{\sigma[k]})+V(r_{(k-1)},R_{\sigma[k-1]})]\right\}a_k + \sum_{\sigma=1}^{P_{\mathrm{bath}}}\left\{\frac{M}{2\hbar^2\Delta\beta_{\mathrm{bath}}^2}(R_\sigma-R_{\sigma-1})^2\right\}b_\sigma, \tag{14}$$

$$G = \sum_{k=1}^{P}\left\{\frac{f_r}{2\Delta\beta^2}-\frac{m}{\hbar^2\Delta\beta^3}(r_k-r_{k-1})^2\right\}a_k^2 + \sum_{\sigma=1}^{P_{\mathrm{bath}}}\left\{\frac{f_R}{2\Delta\beta_{\mathrm{bath}}^2}-\frac{M}{\hbar^2\Delta\beta_{\mathrm{bath}}^3}(R_\sigma-R_{\sigma-1})^2\right\}b_\sigma^2, \tag{15}$$

f_r and f_R are the numbers of partial degrees of freedom for

quantized H and Ni atoms, respectively. a_k and b_σ are coefficients, $\Delta\beta$ and $\Delta\beta_{\text{bath}}$ are defined by $\Delta\beta=\beta/P$, $\Delta\beta_{\text{bath}}=\beta/P_{\text{bath}}$.

C. Adaptive umbrella sampling for $C_{dd}(0)/Q_r$

We rewrite the factor $C_{dd}(0)/Q_r$ in a more detailed form as follows:

$$\frac{C_{dd}(0,s_a^\ddagger,s_b^\ddagger)}{Q_r}=\frac{C_{dd}(0,s_a^0,s_b^0)}{Q_r}\frac{C_{dd}(0,s_a^\ddagger,s_b^\ddagger)}{C_{dd}(0,s_a^0,s_b^0)}, \tag{16}$$

where the term $C_{dd}(0,s_a^0,s_b^0)$ is a property at a particular value of (s_a^0,s_b^0), which is associated with the position of minimum energy, while $C_{dd}(0,s_a^\ddagger,s_b^\ddagger)$ corresponds to the dividing surfaces.

We discretize the Boltzmann operator in $C_{dd}(0)$ and Q_r using the standard procedure as

$$\frac{C_{dd}(0,s_a^0,s_b^0)}{Q_r}=\frac{\int dr_1\cdots\int dr_P\int dR_1\cdots\int dR_{P_{\text{bath}}}\exp\{-\beta\Phi\}\delta(s_0-s_a^0)\delta(s_{P/2}-s_b^0)}{\int dr_1\cdots\int dr_P\int dR_1\cdots\int dR_{P_{\text{bath}}}\exp\{-\beta\Phi\}h(s_0)h(s_{P/2})}, \tag{17}$$

$$\frac{C_{dd}(0,s_a^\ddagger,s_b^\ddagger)}{C_{dd}(0,s_a^0,s_b^0)}=\frac{\int dr_1\cdots\int dr_P\int dR_1\cdots\int dR_{P_{\text{bath}}}\exp\{-\beta\Phi\}\delta(s_0-s_a^\ddagger)\delta(s_{P/2}-s_b^\ddagger)}{\int dr_1\cdots\int dr_P\int dR_1\cdots\int dR_{P_{\text{bath}}}\exp\{-\beta\Phi\}\delta(s_0-s_a^0)\delta(s_{P/2}-s_b^0)}, \tag{18}$$

where Φ is given out by Eq. (12), $h(s_0)$ and $h(s_{P/2})$ stand for that all the PIMC samplings are constrained in the reactant region.

The factor $C_{dd}(0,s_a^0,s_b^0)/Q_r$ is estimated as follows. First, we construct a two-dimensional histogram of the values of $(s_0,s_{P/2})$. Then, we normalize the histogram after hundreds of thousands of samplings have been done. Finally, we can obtain the absolute value of $C_{dd}(0,s_a^0,s_b^0)/Q_r$ at the particular value of (s_a^0,s_b^0).

The other factor in Eq. (16) can be obtained by following the procedure described in Refs. 5 and 8. Basically, we add a global biasing potential $U(x_0,x_{P/2})$ to the discretized action Φ and obtain

$$\frac{C_{dd}^*(0,s_a^\ddagger,s_b^\ddagger)}{C_{dd}^*(0,s_a^0,s_b^0)}=\frac{\int dr_1\cdots\int dr_P\int dR_1\cdots\int dR_{P_{\text{bath}}}\exp\{-\beta\Phi^*\}\delta(s_0-s_a^\ddagger)\delta(s_{P/2}-s_b^\ddagger)}{\int dr_1\cdots\int dr_P\int dR_1\cdots\int dR_{P_{\text{bath}}}\exp\{-\beta\Phi^*\}\delta(s_0-s_a^0)\delta(s_{P/2}-s_b^0)}, \tag{19}$$

where $\Phi^*=\Phi+U(s_0,s_{P/2})$. Since $U(s_0,s_{P/2})$ is a function of only s_0 and $s_{P/2}$, so

$$\frac{C_{dd}^*(0,s_a^\ddagger,s_b^\ddagger)}{C_{dd}^*(0,s_a^0,s_b^0)}=\exp\{-\beta U\}\frac{C_{dd}(0,s_a^\ddagger,s_b^\ddagger)}{C_{dd}(0,s_a^0,s_b^0)}. \tag{20}$$

We can construct a good U by performing an iterative procedure, so as to create a sufficiently flat distribution of $C_{dd}^*(0,s_a,s_b)$ over the domain of (s_a,s_b), i.e.,

$$\frac{C_{dd}(0,s_a^\ddagger,s_b^\ddagger)}{C_{dd}(0,s_a^0,s_b^0)}=\exp\{\beta U_{\text{optimal}}\} \tag{21}$$

Indeed, some of the potential barriers of our systems are very high. In order to accelerate convergence, we add another term PEP (s) (potential energy profile along the reaction path) to the bias potential $U((s_0+s_{P/2})/2,s_0-s_{P/2})=U((s_0+s_{P/2})/2,s_0-s_{P/2})-\text{PEP}((s_0+s_{P/2})/2)$ [we have done a coordinate transformation here from $(s_0,s_{P/2})$ to $((s_0+s_{P/2})/2,s_0-s_{P/2})$] before the execution of the iterative procedure. The PEP (s) is obtained in the following process. First, we fix two reaction coordinate beads $(s_0,s_{P/2},s=s_0=s_{P/2})$ at a special position along the reaction path, then evaluate a potential energy at this position with the Ni atoms relaxed. By repeating the above process at different positions, finally, we can obtain a whole PEP (s) along the reaction path.

The free energy curve can be calculated by

$$F(s)=-k_BT\log C_{dd}(0,s), \tag{22}$$

where $s=s_a=s_b$.

III. MODELS AND COMPUTATIONAL DETAILS

Figures 1 and 2 show H diffusion processes in the nickel crystal with a face-centered-cubic (fcc) lattice structure that we investigate. In the QI calculations, one needs to define the reaction coordinate operators $\hat{s}$ [see Eq. (4)]. For the present system, the hydrogen coordinates are essentially good choices. We thus adopt the following reaction coordinates for different rate processes. In the H diffusion on the Ni(111) surface from a hcp site to a fcc site ($A_{\text{fcc}}\rightleftharpoons A_{\text{hcp}}$), the x coordinate of the H atom is chosen, whose direction is showed in Fig. 1 as the black line connecting the A_{hcp} site to A_{fcc} site. In the H resurfacing from a subsurface octahedral vacancy to the fcc site ($A_{\text{fcc}}\rightleftharpoons Oc_{\text{sub}}$) and from the subsurface tetrahedral vacancy to the hcp site ($A_{\text{hcp}}\rightleftharpoons Te_{\text{sub}}$), the z coordinate of the H atom (vertical to Ni(111) surface) is taken. In the H diffusion between adjacent subsurface octahedral and tetrahedral vacancies ($Oc_{\text{sub}}\rightleftharpoons Te_{\text{sub}}$) and between adjacent interior octahedral vacancy and interior tetrahedral vacancy

($Oc_{inte} \rightleftharpoons Te_{inte}$), the reaction coordinates are the directions perpendicular to the planes of $Ni_1-Ni_2-Ni_3$ and $Ni_4-Ni_5-Ni_6$, respectively.

There is only one full dimensional potential energy surface[20,21] (EAM6) available which we can use in the rate calculations. However, much work has been done to calculate potential barriers for the H/Ni system by using *ab initio* approaches. Because the potential barrier is a key parameter to determine the rates it is necessary to compare the barriers both from the EAM6 and *ab initio* calculations.

For the process of H diffusion on Ni(111) ($A_{hcp} \rightleftharpoons A_{fcc}$), Watson *et al.*[29] and Bhatia and Sholl[30] report the potential barriers to be 3.2 and 2.5 kcal/mol with the density functional theory (DFT), respectively. But, the EAM6 (Ref. 20) predicts a barrier of 2.19 kcal/mol, which is smaller than that of the DFT. Wonchoba and Truhlar[20] explain it by a sizable nonmonotonic H atom coverage dependence.[31–33]

For the process of H resurface from a subsurface octahedral site to a surface fcc site, Sha and Jackson[34] have done a careful work to consider how the relaxation of the lattice affects the barrier using the DFT. They have calculated the potential barriers with three different lattice relaxation schemes. For a rigid lattice, they get a potential barrier of 9.91 kcal/mol. While treating the top two Ni layers with the full relaxation they obtain a dramatically decreased potential barrier of 3.69 kcal/mol, which is in agreement with that of Greeley and Mavrikakis[35] (3.92 kcal/mol), but inconsistent with the calculations by Bhatia and Sholl[30] (5.50 kcal/mol) and Henkelman *et al.*[36] (2.31 kcal/mol). They also consider that the relatively heavy and slow Ni atoms may have little time to fully relax while a light H atom moves between the subsurface and surface site. Thus, they locate the H atom at the subsurface octahedral site, and get a lattice configuration with the minimum energy. With this lattice configuration fixed, they obtain a potential barrier of 5.77 kcal/mol, which agrees with that of the EAM6 (5.86 kcal/mol). Another important factor to affect the barrier may be the subsurface H coverage (θ). It is reported that the barrier changes from 4.15 to 3.46 kcal/mol when the θ changes from 1/3 to 1/9 ML.[37] It is also interesting to note that the barrier is 5.77 kcal/mol in the presence of a methyl group on the surface with the subsurface H coverage $\theta=1/3$ ML,[37] while it is 11.30 kcal/mol with the $\theta=1$ ML.[38]

For the process of H diffusion in interior of bulk Ni, the DFT work[22] predicts a potential barrier of 10.50 kcal/mol ($Oc_{inte} \rightarrow Te_{inte}$), which is agreement with that of the EAM6 (11.15 kcal/mol). However, the DFT predicts a much larger potential barrier for $Te_{inte} \rightarrow Oc_{inte}$ (3.60 kcal/mol) than the one of the EAM6 (1.56 kcal/mol).

From the above comparison with the DFT calculations, the EAM6 looks to be a reasonable full dimensional potential model although its accuracy is questionable to describe the H/Ni with nonzero H coverage due to its single-adatom low-coverage limit.

In the rate calculations for a given rate process, we construct a lattice cell in which all atoms are treated to be movable to incorporate the effect of the crystal fluctuation on the rates. To be concrete, the Ni atoms in the four sides of the bulk metal and at the bottom layers are fixed, the Ni atoms surrounding the reactant and product sites and lying along the reaction path are treated quantum mechanically, and the others are treated classically. It should be noted that the lattice for the interior diffusion process has a structure of sphere, and the outer layers are fixed. The five detailed lattice structures we investigated are listed in Table I.

TABLE I. Lattice structures of H/Ni systems.

Process	Quantized Ni atoms	Classical Ni atoms	Rigid Ni atoms	Total Ni atoms
$A_{fcc} \rightleftharpoons A_{hcp}$	24	47	162	233
$A_{fcc} \rightleftharpoons Oc_{sub}$	31	48	160	239
$A_{hcp} \rightleftharpoons Te_{sub}$	22	42	166	230
$Oc_{sub} \rightleftharpoons Te_{sub}$	33	51	173	257
$Oc_{inte} \rightleftharpoons Te_{inte}$	40	74	214	328

In path integral calculations, the sampling of the discrete paths is performed with the MC method. The numbers of time slices, P and P_{bath} for the degree of freedom of the H and quantized Ni atoms, respectively, are set to $(P, P_{bath}) = (30-40, 6-8)$ in the temperature range of 100–400 K. The number of MC is about $2-6\times10^6$ for computing a single ensemble average. It converges most of the values within 10% statistical errors.

IV. RESULTS

A. Free energy and prefactor

In order to investigate the quantized Ni lattice effect on the rates, we recast the QI formula in Eq. (1) into Arrhenius form, which consists of the free energy and the prefactor

$$k_{QI} = A_{QI} \exp[-\beta \Delta F(\beta)], \tag{23}$$

where the free energy ΔF is defined by

$$\Delta F(\beta) = -1/\beta \log(C_{dd}(0, s_a^{\ddagger}, s_b^{\ddagger})/C_{dd}(0, s_a^0, s_b^0)) \tag{24}$$

and the prefactor has a form

$$A_{QI} = \frac{\sqrt{\pi}}{2} \frac{C_{dd}(0, s_a^0, s_b^0)}{Q_r} \frac{C_{ff}(0, s_a^{\ddagger}, s_b^{\ddagger})}{C_{dd}(0, s_a^{\ddagger}, s_b^{\ddagger})} \frac{\hbar}{\Delta H}. \tag{25}$$

At high temperature limit, it has been shown[7] that ΔF is exactly the same as the free energy barrier used in the variational transition state theory.

Figures 3 and 4 display the calculated free energy profiles for the surface-subsurface and interior processes, respectively, with the quantized, classical, and rigid lattices, respectively, at room temperature (300 K). The corresponding energy barriers, prefactors, and rates are tabulated in Table II.

Figures 3 and 4 clearly show that the classical lattices always reduce the free energy barriers compared with the rigid ones, and the differences of the free energy barriers between the quantized and the classical lattices are not so explicit. For different processes, however, the relaxation effect on the free energies is very different. For hydrogen diffusion on Ni(111), the classical lattice only slightly lowers the free energy barrier, while the barriers decrease more than one-half in subsurface and interior processes. More careful

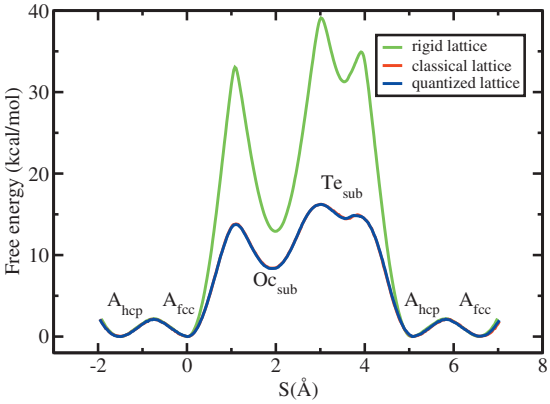

FIG. 3. Free energy profiles with respect to the processes in Fig. 1 at 300 K. The green, the red, and the blue lines correspond to the rigid, classical, and quantized lattices, respectively.

analysis from Fig. 3 reveals that the two preferred Ni(111) surface binding sites, i.e., hcp and fcc hollows have symmetric wells, manifesting that the motions of Ni atoms in the layer beneath the surface have little influence on the surface free energies, despite the fact that the Ni atoms beneath the hcp and fcc hollows have different arrangements. It is also found that the Oc_{sub} site has a deeper well than Te_{sub} site and the well of the Te_{sub} site nearly disappears as quantized Ni atoms are considered. It manifests that the hydrogen at the Te_{sub} site is very unstable, and can easily move to Oc_{sub} site or resurface to hcp site. In the interior processes, although the hydrogen in the Te_{inte} site is much less stable than in the Oc_{inte} site (see Fig. 4), the well at the Te_{inte} site does not disappear. One thus expects that the two-step reaction processes can be used for the reactions from one Oc_{inte} to the other.

Another important feature of the free energy is its temperature dependence. Figure 5 displays the free energy profiles with both H and Ni treated quantum mechanically at several temperatures. Generally speaking, the free energies have a slight difference at 300 and 400 K whereas this difference becomes explicit for 100 and 200 K and the barrier positions move to shallow well directions for asymmetric reactions. The properties can be explained by the hydrogen tunneling effect. At lower temperature the tunneling plays a more important role. Indeed, the barrier heights decrease with decreasing in temperatures except that for $Oc_{\text{sub}} \rightleftharpoons Te_{\text{sub}}$ among 200 to 400 K. This special case may be due to the special structure of the lattice. The thermal average displacements of Ni_1 and Ni_3 (in Fig. 1) vertical to the Ni(111) surface increase with increasing in temperature. Thus, H goes through reaction bottleneck easier at a higher temperature, which makes the barrier decrease. Figure 5 also displays that the free energy barriers of $Oc_{\text{inte}} \rightarrow Te_{\text{inte}}$ change a little in the temperature range of 200–400 K, while those of the $Te_{\text{inte}} \rightarrow Oc_{\text{inte}}$ become shallower and shallower with decreasing in

TABLE II. Free energies and prefactors.

Process (300 K)		ΔF (kcal/mol)	A_{QI} (s^{-1})	k_{QI} (s^{-1})
$A_{\text{fcc}} \rightleftharpoons A_{\text{hcp}}$	a	2.19	1.58(13)	4.07(11)
	b	2.14	1.61(13)	4.49(11)
	c	2.14	1.27(13)	3.47(11)
$A_{\text{fcc}} \rightarrow Oc_{\text{sub}}$	a	33.06	6.87(13)	6.22(−11)
	b	13.79	2.85(13)	2.64(3)
	c	13.75	2.29(13)	2.23(3)
$Oc_{\text{sub}} \rightarrow A_{\text{fcc}}$	a	20.00	6.44(13)	1.83(−1)
	b	5.40	2.10(13)	2.62(9)
	c	5.40	1.72(13)	2.15(9)
$A_{\text{hcp}} \rightarrow Te_{\text{sub}}$	a	34.92	4.29(13)	1.67(−12)
	b	14.94		
	c	14.87		
$Te_{\text{sub}} \rightarrow A_{\text{hcp}}$	a	3.25	5.13(13)	2.28(11)
	b			
	c			
$Oc_{\text{sub}} \rightarrow Te_{\text{sub}}$	a	26.19	5.23(13)	4.31(−6)
	b	7.83	1.86(13)	3.51(7)
	c	7.86	1.45(13)	2.74(7)
$Te_{\text{sub}} \rightarrow Oc_{\text{sub}}$	a	7.83	8.17(13)	1.51(8)
	b	1.75	1.91(13)	1.05(12)
	c	1.73	1.49(13)	8.22(11)
$Oc_{\text{inte}} \rightarrow Te_{\text{inte}}$	a	27.82	5.12(13)	2.86(−7)
	b	11.14	2.50(13)	1.90(5)
	c	11.17	1.75(13)	1.32(5)
$Te_{\text{inte}} \rightarrow Oc_{\text{inte}}$	a	7.07	7.80(13)	6.16(8)
	b	1.52	2.06(13)	1.60(12)
	c	1.47	1.53(13)	1.36(12)

[a]The results for a rigid lattice.
[b]The results for a classical lattice.
[c]The results for a quantized lattice.

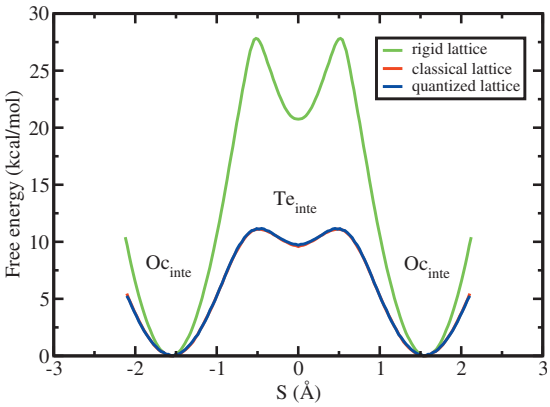

FIG. 4. Free energy profiles with respect to the processes in Fig. 2 at 300 K. The green, the red, and the blue lines correspond to the rigid, classical, and quantized lattices, respectively.

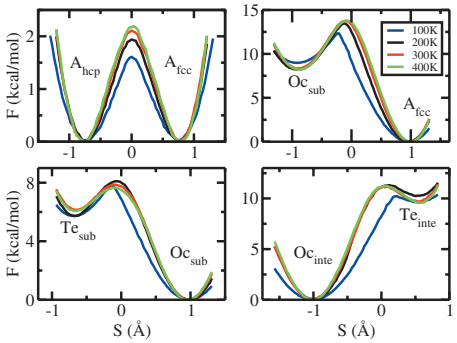

FIG. 5. The temperature dependence of the free energies. The blue, the black, the red, and the green lines correspond to free energy profiles at 100, 200, 300, and 400 K, respectively.

TABLE III. Rate constants (s^{-1}) and diffusion coefficients ($cm^2\ s^{-1}$) for H diffusion on Ni(111) surface. (Powers of 10 are in parentheses.)

		k_{QI}	D_{QI}	$D_{CVT/SCTQ}$[a]	$D_{CVT/SCTQ}$[b]	$\sigma \times D_{CVT/SCTQ}$[b]
100 K	[c]	7.32(9)	1.13(−6)	9.88(−7)		
	[d]	6.72(9)	1.04(−6)		3.46(−8)	1.04(−7)
200 K	[c]	1.09(11)	1.70(−5)	1.39(−5)		
	[d]	1.00(11)	1.55(−5)		1.51(−6)	4.53(−6)
300 K	[c]	4.07(11)	6.30(−5)	7.56(−5)		
	[d]	3.47(11)	5.37(−5)		1.35(−5)	4.05(−5)
400 K	[c]	8.20(11)	1.27(−4)	1.81(−4)		
	[d]	7.56(11)	1.19(−4)		4.60(−5)	1.38(−4)

[a]The results are calculated with POLYRATE (Ref. 39) by ourselves.
[b]The results from Ref. 20 and σ=3.
[c]The results for a rigid lattice.
[d]The results for a quantized lattice.

temperature. The corresponding well depths are 0.47, 1.09, 1.47, and 1.66 kcal/mol at 100, 200, 300, and 400 K, respectively. It manifests that the diffusing H atom may not equilibrate in the interior tetrahedral vacancy at very low temperatures.

Next, we consider the prefactor. Table II shows that the prefactors of the classical lattices are much smaller than those of rigid ones except for the process of H diffusion on Ni(111), and the prefactors of quantized lattices are always smaller than those of classical ones, but their amplitudes have the same order, which is consistent with our previous work.[1] This may be explained by the fact that the quantum motions of the surface atoms can induce the dissipative effect on the tunneling degrees of freedom because the prefactor essentially incorporates the dynamical effect. It is well known that pure dissipation in the overdamping regime always hinders the reaction rates for a given reaction barrier. The present results thus are consistent with above analysis. However, the rates are determined by both the prefactor and free energy barrier the tunneling coordinate sees. If the contribution of the modified free energy profile to the rate overwhelms that from the dissipative effect, the rate may dominantly depend on the property of the free energy barrier. The rates listed in Table II show these properties. For the process of H diffusion on Ni(111) surface, the rate with a quantized lattice is smaller than the ones on a rigid lattice. This is because the free energy barrier changes a little, and the rate mainly depends on the prefactor. However, other processes show an opposite tendency, i.e., the rates with the quantized lattice are much larger (several orders) than those with the rigid lattice due to the dramatic differences of the free energy barriers in these cases. Although the free energy profiles for quantized and classical lattices are similar, the quantized lattice lowers the rates by 20%–40%.

B. Rate constants and diffusion coefficients

Under the Markovian assumption that the hydrogen can only jump to its nearest neighbor site and that successive jumps are uncorrelated, the diffusion coefficient can be expressed in terms of the rates

$$D(T) = \frac{\lambda^2 \sigma}{2d} k_{QI}(T), \tag{26}$$

where T is the temperature, λ is the distance between reactant and product minimum-energy sites, σ is a symmetry factor equal to the number of equivalent pathways from the reactant site to product site, and d is the dimensionality of the process. Here, we calculate diffusion coefficients only for two processes, that are H diffusion on Ni(111) surface and H diffusion in interior of bulk nickel. The parameters λ, σ, d for these two processes are $\sqrt{6}R_0/6$, 3, 2, and $R_0/\sqrt{2}$, 8, 3, respectively. Here, R_0 is the lattice constant equal to 3.52 Å.

1. H diffusion on Ni(111) surface

Table III displays the rate constants and diffusion coefficients for H diffusion on Ni(111) surface with temperatures ranging from 100 to 400 K, where the cases a and b correspond to the rigid and quantized lattice, respectively, and the hydrogen atom is always treated quantum mechanically in the calculations. Despite quantized lattice lowers the free energy barrier that the reaction path sees (see Fig. 3), which has a tendency to enhance the rates, the rates are decreased in a wide temperature regime. This result is similar to that on Ni(100).[1] Thus, one may expect that the dynamics of the quantized lattice slightly influences the barrier of the hydrogen diffusion on Ni surface, and its overall effect is to hinder the rates and diffusion coefficients because of smaller prefactors comparing with a rigid one. In such a case, the adiabatic reaction path way method or Kramers rate theory may be applicable because the reaction potential barrier does not change too much as quantized lattice is incorporated.

Table III also lists the CVT/SCTQ results on a quantized lattice obtained by Wonchoba and Truhlar[20] and those on a rigid lattice calculated with POLYRATE (Ref. 39) by ourselves. In order to compare with the QI results, we have multiplied the symmetric factor σ(=3) to the Wonchoba's CVT/SCTQ data. Qualitatively and quantitatively, the CVT/SCTQ results are consistent with the QI ones quite well, i.e., the CVT/SCTQ also predicts that quantized lattice can hinder the rates, and the predicted diffusion coefficients are very close to the QI results except for low temperatures (100 and 200 K), where the QI data are greater than the CVT/SCTQ ones.

TABLE IV. Rate constants (unit: s^{-1}; powers of 10 are in parentheses) for resurfacing and subsurface processes.

	100 K	200 K	300 K	400 K	600 K
$A_{fcc} \rightarrow Oc_{sub}$ [a]	3.81(−14)	1.14(−1)	2.23(3)	5.48(5)	2.43(8)
$A_{fcc} \rightarrow Oc_{sub}$ [b]	1.09(−15)	1.23(−1)	9.72(3)	3.36(6)	1.16(9)
$Oc_{sub} \rightarrow A_{fcc}$ [a]	1.17(6)	4.59(7)	2.15(9)	1.23(10)	1.02(11)
$Oc_{sub} \rightarrow A_{fcc}$ [b]	1.62(5)	7.36(7)	2.93(9)	2.33(10)	2.15(11)
$Oc_{sub} \rightarrow Te_{sub}$ [a]	2.78(−4)	1.99(4)	2.74(7)	1.18(9)	2.49(10)
$Te_{sub} \rightarrow Oc_{sub}$ [a]	7.24(8)	4.68(10)	8.22(11)	2.00(12)	4.13(12)

[a]The QI results with a quantized lattice.
[b]The CVT/SCT results from Ref. 20.

This difference requires further to improve the tunneling probability in the CVT/SCTQ in the deep tunneling regime.

2. Resurfacing and subsurface processes

In the resurfacing process, $Te_{sub} \rightarrow A_{hcp}$ does not show an obvious barrier (see Fig. 3), especially at low temperatures, as the lattice atoms are treated quantum mechanically. This step thus can be thought as a barrierless process. Table IV tabulates the rate constants for the other resurfacing and subsurface processes in the temperature range of 100–600 K. We also list the available CVT/SCT results for $Oc_{sub} \rightarrow A_{fcc}$ and its reverse reaction.[20] Again, the CVT/SCT rates are close to the QI rates except at 100 K. However, an explicit difference for the temperature dependence of the rates is found by two approaches compared with the situation of the hydrogen diffusion on Ni surface.

Several experimental and theoretical investigations[40,41,38,37] have demonstrated that subsurface hydrogen is much more reactive than surface hydrogen in heterogeneous catalysis. However, its favorable resurfacing paths are not clear yet. Despite we have considered all possible paths in the calculations, here, we focus on the dominant resurfacing channels. As it is mentioned, Te_{sub} is very unstable because of the shallow well. Thus, the H in the subsurface is mostly located at Oc_{sub} site. From this site to the surface, the rate determined steps are $Oc_{sub} \rightarrow A_{fcc}$ and $Oc_{sub} \rightarrow Te_{sub}$. The data in the Table IV reveal that the rate ratios of $Oc_{sub} \rightarrow A_{fcc}$ to $Oc_{sub} \rightarrow Te_{sub}$ are 4.2×10^9, 2300, 78, 10, and 4 at 100, 200, 300, 400, and 600 K, respectively. Although the barriers for these two channels are close to each other, surprisingly, a huge difference of the rates exists with respect to temperatures. It can be understood from the fact that the rates are determined by the tunneling at low temperatures where the $Oc_{sub} \rightarrow A_{fcc}$ has a narrower barrier width, while the rates are dominated by jumping the barriers at high temperatures where there are similar barriers for both the channels. More interestingly, one may expect to control the resurfacing processes by temperatures. When the H is only required to resurface to the A_{fcc} site one can lower temperature, and high temperature will help resurface the H to both sites A_{fcc} and A_{hcp}. In the present calculations, A_{hcp} site can be explicitly resurfaced by the subsurface H at 600 K.

It is noted that an experiment[42] has measured the resurfacing of the trapped bulk H and found the desorption rate peaks occur between 180 and 220 K. Sha and Jackson[34] has successfully fitted the experiment by using the rates obtained from the transition state theory based on the DFT potential barrier of the rigid lattice. However, compared with the resurfacing rates from Sha and Jackson, our results on the quantized lattice are eight orders of magnitude larger. This large difference is mainly due to the different potential barrier heights, which are 5.86 and 9.91 kcal/mol for EAM6 and Sha's calculation, respectively. The previous DFT work of Michaelides *et al.*[38] and Ledentu *et al.*[37] shows that the barrier height will be increased with increasing the subsurface H coverage, which reflects that the high subsurface H coverage restrains the lattice from relaxing. Because EAM6 is constructed for the single-adatom low-coverage limit, EAM6 needs to be further improved to incorporate H coverage effect to better explain experiment.

3. H diffusion in interior of bulk Ni

In the interior of bulk Ni, the two most stable sites to cage H are symmetric octahedral vacancies (see Fig. 2). The H diffusion between them has been measured experimentally.[43–46] Several theoretical calculations have also been proposed to investigate this diffusion process. Wimmer *et al.*[22] calculate the diffusion coefficient via two step reactions $Oc_{inte} \rightarrow Te_{inte} \rightarrow Oc_{inte}$ by using a transition state theory together with accurate *ab initio* energies while Wonchoba and Truhlar[20] consider the kinetic step as a direct process with a double maximum barrier and calculate the diffusion coefficient using the CVT/SCT. In the present QI calculations, Fig. 5 has explicitly shown that the free energies have a well at the tetrahedral site from 200 to 400 K. It is thus reasonable to assume that the diffusing H atom temporarily equilibrates in the tetrahedral site before jumping forward or backward to a neighboring octahedral site. The two kinetic steps are good assumption for the diffusion between two octahedral vacancies. The free energy well, however, becomes very shallow at 100 K. In this case, the direct reaction from the octahedral site to the other one may be acceptable. Here, we only calculate the rates via the two kinetic steps. The rates are 2.94×10^1, 1.32×10^5, and 1.18×10^7 ($cm^2\ s^{-1}$) for $Oc_{inte} \rightarrow Te_{inte}$, and 8.37×10^{11}, 1.36×10^{12}, and 1.82×10^{12} ($cm^2\ s^{-1}$) for $Te_{inte} \rightarrow Oc_{inte}$, at 200, 300, and 400 K, respectively. The diffusion coefficients thus can be obtained by using Eq. (26) from the above rates.

The temperature dependence of the diffusion coefficients are commonly fitted to the Arrhenius equation

TABLE V. Arrhenius parameters for H diffusion in interior of bulk Ni. (Powers of 10 are in parentheses.)

		D_0 ($cm^2\ s^{-1}$)	E_a (kcal/mol)
Present[a]	200–400 K	3.93(−3)	10.26
Wonchoba[b] (theoretical data)	295–300 K	1.3(−3)	11.1
	300–627 K	7.8(−4)	10.9
	627–1650 K	4.4(−4)	10.2
Wimmer[c] (theoretical data)	273–1000 K	3.84(−2)	10.92
Yamakawa[d] (experimental data)	220–350 K	1.9(−3)	8.89
Ebisuzaki[e] (experimental data)	470–690 K	5.22(−3)	9.56
Eichenauer[f] (experimental data)	660–930 K	6.73(−3)	9.47
Katz[g] (experimental data)	670–1270 K	7.04(−3)	9.43

[a]The QI diffusion coefficients for $Oc_{\text{inte}} \rightarrow Oc_{\text{inte}}$.
[b]Results from Ref. 20.
[c]From Ref. 22.
[d]From Ref. 46.
[e]From Ref. 44.
[f]From Ref. 43.
[g]From Ref. 45.

$$D(T) = D_0 \exp\left[\frac{-E_a}{RT}\right], \tag{27}$$

where R is the gas constant, D_0 and E_a are the pre-exponential factor and the activation energy, respectively. The QI calculations predict $D_0 = 3.93 \times 10^{-3}$ $cm^2\ s^{-1}$ and $E_a = 10.26$ kcal/mol. In the calculations, the rates of $Oc_{\text{inte}} \rightarrow Te_{\text{inte}}$ are used to obtain the diffusion coefficients because this process is much slower than that of $Te_{\text{inte}} \rightarrow Oc_{\text{inte}}$ and it determines the total reaction rates.

Table V tabulates the pre-exponential factors and activation energies coming from available experiments and theories. It is found that both D_0 and E_a from the QI calculations are very close to Ebisuzki's experimental data[44] where $D_0 = 5.22 \times 10^{-3}$ $cm^2\ s^{-1}$ and $E_a = 9.56$ kcal/mol. Further tracking down the comparisons with experiments is nontrivial because the accuracy of the diffusion coefficients is much dependent of the potential energy surface. However, we may make a quantitative comparison for the QI and CVT/SCT results. With use of the diffusion coefficients from 295 to 300 K obtained by the CVT/SCT, Wonchoba and Truhlar[20] predict 11.1 kcal/mol for E_a, and 1.3×10^{-3} $cm^2\ s^{-1}$ for D_0, respectively. These values are observably different from the QI calculations. E_a and D_0 are 0.8 kcal/mol larger and three times smaller than those from the QI calculations, respectively. The origin of these differences can be explained by that Wonchoba and Truhlar[20] have treated the processes $Oc_{\text{inte}} \rightarrow Te_{\text{inte}}$ and $Te_{\text{inte}} \rightarrow Oc_{\text{inte}}$ as a single kinetic step rather than as two kinetic steps, which results in a much longer tunneling path than that of the two steps. Comparing with the results reported by Wimmer *et al.*,[22] the activation energy is about 0.6 kcal/mol larger than the present one, and the pre-exponential factor is ten times larger, which is also larger than all available experimental data. These differences may come from both the different potential energy surfaces and rate methods.

V. CONCLUDING REMARKS

We have evaluated the free energy profiles along the reaction paths, temperature dependence of free energies, rates, and diffusion coefficients for five processes of H/Ni system using the QI approximation with a potential energy surface based on the embedded diatomics-in-molecules method.

For the process of hydrogen diffusion on Ni(111) surface, we find that the free energies at the A_{fcc} and the A_{hcp} binding sites exhibit a symmetric double well despite the lattice structures beneath these two sites are different. One thus expects that the dynamics of these different structures has little effect on the hydrogen diffusion on the surface.

For the processes of surface-to-subsurface transport and resurface, the quantized free energy profiles along the reaction paths show that the hydrogen at Oc_{sub} site is much more stable than the one at Te_{sub} site, especially at low temperatures where the free energy well at Te_{sub} for stabling the hydrogen nearly disappears. From the QI rates, it is found that the hydrogen is more likely to penetrate into bulk nickel from a A_{fcc} binding site on Ni(111) surface than a A_{hcp} binding site, and the hydrogen in the Oc_{sub} site is preferred to resurface through the path $Oc_{\text{sub}} \rightarrow A_{\text{fcc}}$ at low temperature, however, both the paths $Oc_{\text{sub}} \rightarrow A_{\text{fcc}}$ and $Oc_{\text{sub}} \rightarrow Te_{\text{sub}} \rightarrow A_{\text{hcp}}$ are possible at high temperatures. Thus, temperature can be taken as an important control parameter to determine the resurface paths.

For the process of hydrogen diffusion in interior of bulk Ni, the diffusion mechanism of $Oc_{\text{inte}} \rightarrow Oc_{\text{inte}}$ process may depend on temperature. At high temperatures, the hydrogen at the intermediate site Te_{inte} has an explicit stable structure observed from the quantized free energy profile along the reaction path, while the free energy wells for the stability become flat at very low temperatures. Thus, $Oc_{\text{inte}} \rightarrow Oc_{\text{inte}}$ should be divided into two individual kinetic steps $Oc_{\text{inte}} \rightarrow Te_{\text{inte}}$ and $Te_{\text{inte}} \rightarrow Oc_{\text{inte}}$ at high temperatures, while it can be considered as a direct step at low temperatures. It is noted that the present conclusion seems at variance with conventional idea based on the adiabatic potential energy the reaction path sees, which predicts that low temperature always help to stable the hydrogen in the Te_{inte}. There is actually no inconsistency. This is because the quantized motions of the H and Ni atoms tend to lower the barriers due to the tunneling comparing with stationary potential barriers, and a stable structure based on the stationary potential may become unstable as the tunneling effect is large enough.

The relaxation of Ni atoms play a significantly rule in the determination of the free energy barriers. Despite it does not change the barrier too much for H diffusion on Ni(111) surface, it dramatically lowers the free energy barriers for H transport in interior of bulk Ni. The present simulations shows that this decreasing can increase rates by several orders. Compared with classical motions of lattice atoms, the quantum motions always hinder the rates via the smaller prefactors. It may be explained by the pure quantum dissipative effect, i.e., the quantum motions of the metallic atoms can induce the dissipation on the tunneling degrees of freedom and the rates will decrease with increasing in dissipa-

tion. In general, the quantized lattices lowers the rates by 20%–40% compared with the classical lattices.

ACKNOWLEDGMENTS

This work is partially supported by the National Science Foundation of China (Grant Nos. 20773115 and 20833004), National Key Basic Research Foundation Program of China (Grant No. 2007CB815204), and Research Fund for the Doctoral Program of Higher Education of China (Grant No. 200803840009).

[1] W. Wang and Y. Zhao, J. Chem. Phys. **130**, 114708 (2009).
[2] W. H. Miller, Y. Zhao, M. Ceotto, and S. Yang, J. Chem. Phys. **119**, 1329 (2003).
[3] W. H. Miller, J. Chem. Phys. **62**, 1899 (1975).
[4] S. Coleman, Phys. Rev. D **15**, 2929 (1977).
[5] T. Yamamoto and W. H. Miller, J. Chem. Phys. **120**, 3086 (2004).
[6] Y. Zhao, T. Yamamoto, and W. H. Miller, J. Chem. Phys. **120**, 3100 (2004).
[7] W. Wang, S. Feng, and Y. Zhao, J. Chem. Phys. **126**, 114307 (2007).
[8] T. Yamamoto and W. H. Miller, J. Chem. Phys. **122**, 044106 (2005).
[9] Y. Fukai and H. Sugimoto, Adv. Phys. **34**, 263 (1985).
[10] J. D. Doll and A. F. Voter, Annu. Rev. Phys. Chem. **38**, 413 (1987).
[11] R. Gomer, Rep. Prog. Phys. **53**, 917 (1990).
[12] P. Saalfrank and W. H. Miller, Surf. Sci. **303**, 206 (1994).
[13] E. G. Seebauer and C. E. Allen, Prog. Surf. Sci. **49**, 265 (1995).
[14] J. V. Barth, Surf. Sci. Rep. **40**, 75 (2000).
[15] J. Greeley, J. K. Norskov, and M. Mavrikakis, Annu. Rev. Phys. Chem. **53**, 319 (2002).
[16] M. Nishijima, H. Okuyama, N. Takagi, T. Aruga, and W. Brenig, Surf. Sci. Rep. **57**, 113 (2005).
[17] A. Pundt and R. Kirchheim, Annu. Rev. Mater. Res. **36**, 555 (2006).
[18] T. N. Truong and D. G. Truhlar, J. Chem. Phys. **93**, 2125 (1990).
[19] R. Baer and R. Kosloff, J. Chem. Phys. **106**, 8862 (1997).
[20] S. E. Wonchoba and D. G. Truhlar, Phys. Rev. B **53**, 11222 (1996).
[21] R. Baer, Y. Zeiri, and R. Kosloff, Phys. Rev. B **55**, 10952 (1997).
[22] E. Wimmer, W. Wolf, J. Sticht, and P. Saxe, Phys. Rev. B **77**, 134305 (2008).
[23] B. J. Berne and D. Thirumalai, Annu. Rev. Phys. Chem. **37**, 401 (1986).
[24] D. M. Ceperley, Rev. Mod. Phys. **67**, 279 (1995).
[25] C. Chakravarty, Int. Rev. Phys. Chem. **16**, 421 (1997).
[26] M. Mezei, J. Comput. Phys. **68**, 237 (1987).
[27] R. W. W. Hooft, B. P. van Eijck, and J. Kroon, J. Chem. Phys. **97**, 6690 (1992).
[28] C. Bartels and M. Karplus, J. Comput. Chem. **18**, 1450 (1997).
[29] G. W. Watson, R. P. K. Wells, D. J. Willock, and G. J. Hutchings, J. Phys. Chem. B **105**, 4889 (2001).
[30] B. Bhatia and D. S. Sholl, J. Chem. Phys. **122**, 204707 (2005).
[31] T. S. Lin and R. Gomer, Surf. Sci. **255**, 41 (1991).
[32] A. Lee, X. D. Zhu, A. Wong, and L. Deng, Phys. Rev. B **48**, 11256 (1993).
[33] T. R. Mattsson and G. Wahnström, Phys. Rev. B **51**, 1885 (1995).
[34] X. Sha and B. Jackson, Chem. Phys. Lett. **357**, 389 (2002).
[35] J. Greeley and M. Mavrikakis, Surf. Sci. **540**, 215 (2003).
[36] G. Henkelman, A. Arnaldsson, and H. Jónsson, J. Chem. Phys. **124**, 044706 (2006).
[37] V. Ledentu, W. Dong, and P. Sautet, J. Am. Chem. Soc. **122**, 1796 (2000).
[38] A. Michaelides, P. Hu, and A. Alavi, J. Chem. Phys. **111**, 1343 (1999).
[39] R. Steckler, W.-P. Hu, Y.-P. Liu, G. C. Lynch, B. C. Garrett, A. D. Isaacson, V. S. Melissas, D. Lu, T. N. Truong, S. N. Rai, G. C. Hancock, J. G. Lauderdale, T. Joseph, and D. G. Truhlar, Comput. Phys. Commun. **88**, 341 (1995).
[40] A. D. Johnson, S. P. Daley, A. L. Utz, and S. T. Ceyer, Science **257**, 223 (1992).
[41] S. P. Daley, A. L. Utz, T. R. Trautman, and S. T. Ceyer, J. Am. Chem. Soc. **116**, 6001 (1994).
[42] A. D. Johnson, K. J. Maynard, S. P. Daley, Q. Y. Yang, and S. T. Ceyer, Phys. Rev. Lett. **67**, 927 (1991).
[43] W. Eichenauer, W. Löser, and H. Witte, Z. Metallk. **56**, 287 (1965).
[44] Y. Ebisuzaki, W. J. Kass, and M. O'Keeffe, J. Chem. Phys. **46**, 1378 (1967).
[45] L. Katz, M. Guinan, and R. J. Borg, Phys. Rev. B **4**, 330 (1971).
[46] K. Yamakawa, J. Phys. Soc. Jpn. **47**, 114 (1979).